IOP PUBLISHING JOURNAL OF PHYSICS D: APPLIED PHYSICS

J. Phys. D: Appl. Phys. **42** (2009) 215101 (6pp) doi:10.1088/0022-3727/42/21/215101

Electromagnetic interaction between a metallic nanoparticle and surface in tunnelling proximity—modelling and experiment

J Mitra, Lei Feng, Michael G Boyle and P Dawson

Centre for Nanostructured Media, School of Mathematics and Physics, Queen's University, Belfast BT7 1NN, UK

E-mail: j.mitra@qub.ac.uk

Received 16 June 2009, in final form 12 August 2009
Published 13 October 2009
Online at stacks.iop.org/JPhysD/42/215101

Abstract

We simulate the localized surface plasmon resonances of an Au nanoparticle within tunnelling proximity of an Au substrate. The results demonstrate that the calculated resonance energies can be identified with those experimentally detected for light emission from the tip–sample junction of a scanning tunnelling microscope. Relative to the modes of an isolated nanoparticle these modes show significant red-shifting, extending further into the infrared with increasing radius, primarily due to a proximity-induced lowering of the effective bulk plasmon frequency. Spatial mapping of the field enhancement factor shows an oscillatory variation of the field, absent in the case of a dielectric substrate; also the degree of localization of the modes, and thus the resolution achievable electromagnetically, is shown to depend primarily on the nanoparticle radius, which is only weakly dependent on wavelength.

S Animation S1 and Figure S2.

1. Introduction

The electromagnetic interaction of light with noble metal nanostructures is of considerable current interest both from a technological and from a fundamental physics point of view. The strong electric field enhancement associated with localized surface plasmon (LSP) excitations on such nanostructures plays a key role in various fields such as surface enhanced Raman spectroscopy (SERS) [1], biological sensing [2, 3] and targeted drug delivery [4]. As observed in the case of SERS and tip enhanced Raman spectroscopy (TERS), if the energy of the LSP modes can be pre-tuned to the absorption band of the sample under study, it leads to dramatic enhancement of the signal. The plasmonic interaction between individual noble metal nanostructures or with the substrate is significantly altered in the presence of molecules (due to a change in the dielectric environment [5]) and any detectable change in the interaction paves the way for molecular biological sensing [2], potentially down to a single molecule level. Similarly, recent results show that different molecules attached to nanorods of different sizes/shapes can be selectively released by irradiation tuned to the surface plasmon resonance of a nanorod of a particular geometry [6]. Other novel applications of LSPs pertain to near-field focusing for sub-wavelength imaging [7] and plasmonic nanolithography [8, 9]. In all cases the primary advantage of using nanostructures is the highly localized, strong electric field enhancement and the fact that their electromagnetic interaction characteristics can be accurately controlled through a change in geometric properties. Thus, it is vital to understand the interaction of electromagnetic fields with nanostructures, leading to LSP excitation. The key characteristics of the LSPs of a metallic nanoparticle—energy, field enhancement and field distribution—are determined by its geometry, dielectric properties, the environment and, crucially, its proximity to other (metallic) structures or substrate, the issue specifically addressed in this work.

In this study we focus on junction-based optical spectroscopy techniques such as light emission from scanning

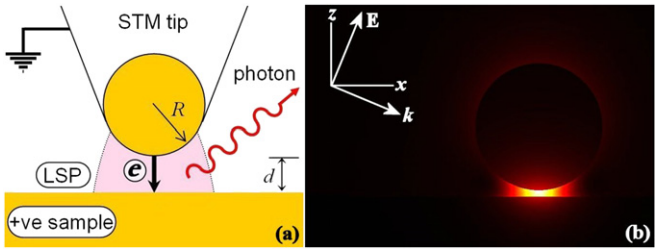

Figure 1. (*a*) Schematic of the STM tip–sample junction and the light emission process, (*b*) The *xz* plane snapshot of the calculated electric field distribution around a 10 nm radius Au nanoparticle near a 30 nm thick Au substrate for $\lambda = 900$ nm. The propagation vector k is 20° to the x-axis.

(This figure is in colour only in the electronic version)

tunnelling microscopy (LESTM) and TERS. Both exploit the high electric field enhancement associated with the LSPs of a 'nanocavity' (formed between a metallic tip in close proximity to a substrate) and have been used to probe the energetics of nanoentities placed within, from molecules to nanowires. Enhanced sensitivity, originating with the strong field enhancement, is combined with high spatial resolution that stems from the localized nature of the LSPs in the nanocavity. TERS has shown chemical identification of single molecules [10] and nanowires [11] with a lateral resolution of 10–20 nm, while chemical sensing in LESTM has been performed with a resolution of a few nanometres [12]. The geometry of these experiments is treated here as that of a metal nanoparticle (representing the tip) in close proximity to a substrate (figure 1(*a*)). A number of theoretical studies have investigated the LSP modes of both the tip–sample [13–15] and the nanoparticle–substrate system [16–18]; however, they have tended to be either pure modelling exercises (i.e. no direct comparison with experiment is drawn) and/or do not mimic the specific conditions of LESTM. In this investigation we extend the analysis of such studies by modelling the exact conditions of the LESTM setup (i.e. tip and sample in *tunnelling* proximity) and by producing detailed correlation of the modelled data with experiment.

We have applied finite element modelling to identify the LSP modes of a single spherical Au nanoparticle (of radius R), within tunnelling proximity (gap dimension d) of a planar Au substrate. Using plane wave optical excitation, individual LSP resonances are evidenced as peaks in plots of the electric field enhancement factor (E_f) versus wavelength (λ) for the nanocavity. Using a simple reciprocity argument, LSP modes excited in the nanocavity should couple to waves propagating away from the nanocavity region, with spectra of the outcoupled light exhibiting peaks at energies corresponding to those of the resonant LSPs. Here we make the connection to LESTM (figure 1(*a*)), in which tunnel current fluctuations excite the LSP modes of the tip–sample nanocavity [19–21], and subsequently decay, giving rise to broadband emission with characteristic peaks at the modal energies; optically, the nanoparticle in the modelling equates to the scanning tunnelling microscope (STM) tip and should be of closely comparable radius. Although the excitation mechanism is different in the two scenarios, i.e. optical in the modelling and electronic in the experiment, the energies of the LSP modes (being purely a function of the nanocavity geometry and dielectric properties of the environment) remain unchanged.

In the following we demonstrate a close match between the LSP modal energies obtained in the experimental and simulated results. While confirming a large red-shift of the LSP modal energies with increasing R the results also elucidate the spatial localization of E_f in the nanocavity. We consider the limit of the lateral resolution achievable in LESTM and the conditions required for its realization. These findings are highly relevant to the design of any junction based optical spectroscopy.

2. Material and methods

The wavelength-dependent response of the nanoparticle–substrate system was simulated using a commercial 3D finite element modelling package (COMSOL Multiphysics 3.3a). The simulation domain comprises a single spherical nanoparticle (of radius R) separated from a square plane, of side $10R$ and thickness 30 nm, by a gap with $d = 0.6$ nm (a typical value for STM). A thickness larger than the optical skin depth of Au is chosen to exclude any thickness dependent effects of the LSP excitation energies [16]. Here, we assume that the Au nanoparticle and substrate are characterized by the Drude dielectric function [22] given by $\varepsilon_{Au} = \{1 - \omega_p^2/(\omega^2 + \gamma^2)\} + i\{\gamma\omega_p/(\omega^2 + \gamma^2)\}$, where $\hbar\omega_p$ is the bulk plasmon frequency, ω is the angular frequency and γ is the damping term. The assumption is valid for wavelengths (energies) longer (lower) than the interband transitions in Au, thus only for $\lambda > 500$ nm [23]. The surrounding medium is considered as free space ($\varepsilon = 1.00$). The model is non-uniformly meshed ensuring approximately 10 mesh points between the nanoparticle and the substrate. The simulation calculates the local electromagnetic field at every mesh point with an incident p-polarized plane wave (figure 1(*b*), propagation vector, $\boldsymbol{k}$ tilted at 20° below the x-axis) for the wavelength range 500–1500 nm at 10–20 nm intervals. The incident electric field strength is scaled to unity so that the calculated field represents E_f. The values used for $\hbar\omega_p$ and γ are 3.6 eV and 0.1 eV, respectively; we comment further on the value of $\hbar\omega_p$ in the discussion of the results.

The experimental setup comprises a Digital Instruments Nanoscope-E STM housed in an environment controlled enclosure, operated with Au tips on Au(1 1 1) surfaces. In order to preclude the effects of the presence of atmospheric water vapour on LESTM [5] the relative humidity of the enclosure was maintained below 10%, while acquiring the data presented here. We present emission spectra corresponding to three Au tips (prepared by electrochemical etching of an Au wire [24]) with tip end radii of ~10, 25 and 80 nm, as estimated from scanning electron microscope images. Figure 2(inset) shows the image of a 10 nm tip. Au(1 1 1) surfaces were freshly prepared by flame annealing 200 nm thick Au films. The light output was collected by two 800 μm core, low-OH^- content optical fibres, positioned ~1 mm from the tip–sample region and fed to an Acton Research SpectraPro 275 spectrometer fitted with an Andor DU420-OE charge

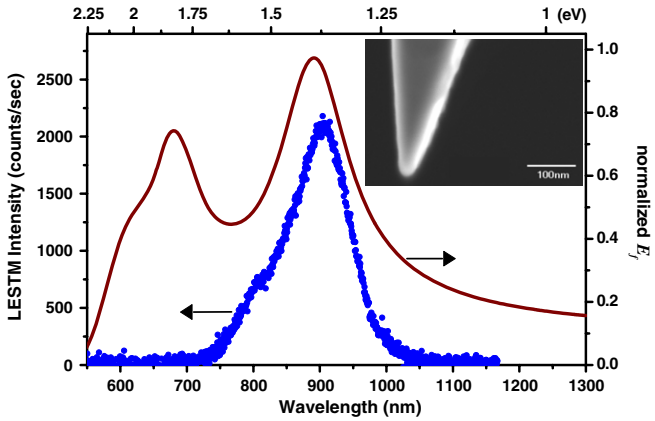

Figure 2. (●) STM light emission spectrum for tip of $R \sim 10$ nm for $V_b = 1.75$ V ($\lambda_{min} \sim 709$ nm) and corresponding simulation showing normalized E_f as a function of wavelength (energy). The inset shows the SEM image of the etched tip.

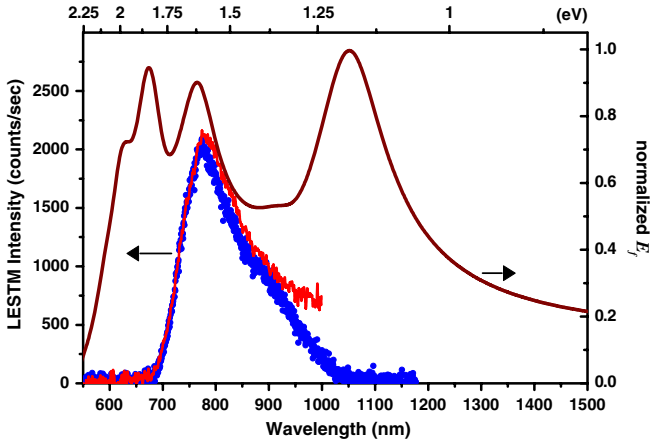

Figure 3. (●) STM light emission spectrum for tip of $R \sim 25$ nm and (——) spectrum after correction for the efficiency of the spectrometer–detector setup for $V_b = 1.80$ V ($\lambda_{min} \sim 688$ nm). Corresponding simulation showing normalized E_f as a function of wavelength (energy).

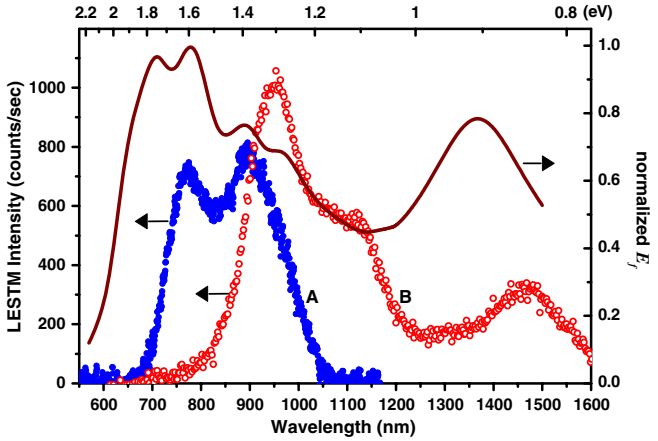

Figure 4. (●) STM light emission spectrum for tip of $R \sim 80$ nm for $V_b = 1.80$ V ($\lambda_{min} \sim 688$ nm), and corresponding simulation showing E_f as a function of wavelength (energy). (○) STM light emission spectrum for a tip of $R \sim 100$ nm with $V_b = 1.85$ V, from [21]. The intensity of spectrum B is scaled down by a factor of 3 to make it comparable to spectrum A.

coupled device (CCD) camera to record the emission spectrum (overall detection range 400–1000 nm). In this setup the long wavelength cutoff of the recorded spectra is dictated by the CCD camera ($\lambda_{max} \sim 1000$ nm), while the short wavelength cutoff, λ_{min}, is determined by the applied sample bias (V_b) according to the quantum cutoff condition, $hc/\lambda_{min} = eV_b$, thus allowing emission only at energies lower than V_b. Theoretical understanding of LESTM shows that the emission is weighted by the factor[1] $(1 - \hbar\omega/eV_b)$ for $\hbar\omega \leqslant eV_b$ [17, 19]. Owing to this, excitation of LSP modes at higher energies (especially close to V_b) is highly suppressed in comparison with those at lower energies. The spectral data presented here were acquired for a positive sample bias of $\sim$1.8 V ($\lambda_{min} \approx 688$ nm) and 10 nA tunnel current. Each spectrum was obtained by averaging ten 60 s exposures. The spectra are not corrected for the wavelength dependent efficiency of the detection setup; such correction changes the peak positions by less than 10 nm (illustrated in figure 3, where the shift is actually < 5 nm).

3. Results and discussion

Figures 2–4 plot the LESTM spectra from tips with end radii $R = 10$, 25 and 80 nm with the corresponding simulation data showing plots of the normalized E_f, at a point (0.1 nm below) directly below the nanoparticle. The E_f versus λ plot in figure 2 (for nanoparticle with $R \sim 10$ nm) shows two peaks at $\lambda \sim 680$ nm and at $\lambda \sim 895$ nm, which we refer to as the first ($\hbar\omega_1 = 1.82$ eV) and zero order ($\hbar\omega_0 = 1.38$ eV) LSP resonances, respectively. The first order peak, which falls within the detection range of this setup, is evidenced by the peak at $\lambda \sim 900$ nm in the LESTM spectra (for tip with $R \sim 10$ nm). It is worth noting that for this *sharp* tip the present simulation and experimental results [21] indicate the absence of any further LSP resonances at longer wavelengths, thus the lowest energy peak is identified above as the zero order resonance.

[1] The factor originates from the tunnel current power spectral density.

The simulation results in figure 3 (for $R \sim 25$ nm) exhibit three distinct peaks at $\lambda \sim 675$ nm, 765 nm and 1059 nm, corresponding to the second ($\hbar\omega_2 = 1.83$ eV), first ($\hbar\omega_1 = 1.62$ eV) and zero ($\hbar\omega_0 = 1.17$ eV) order LSP resonances, respectively. Emission corresponding to the first order mode is detected in the LESTM spectrum with a peak at $\lambda \sim 770$ nm. The E_f plot indicates that the overall LSP resonances have red shifted with the lowest energy mode shifting to 1059 nm, beyond the detection range of the CCD camera.

Simulation results presented in figure 4 (for $R \sim 80$ nm) exhibit five distinct peaks at $\lambda \sim 708$ nm, 779 nm, 891 nm, 965 nm and 1340 nm, corresponding to the fourth ($\hbar\omega_4 = 1.75$ eV), third ($\hbar\omega_3 = 1.59$ eV), second ($\hbar\omega_2 = 1.39$ eV), first ($\hbar\omega_1 = 1.28$ eV) and zero ($\hbar\omega_0 = 0.92$ eV) order LSP resonances. The LESTM results (spectrum A in figure 4) from the third tip ($R \sim 80$ nm) show two peaks at 774 nm and 893 nm, corresponding to the third and second order LSP

resonances seen in E_f, which fall within the detection range. Although the fourth order mode at $\hbar\omega_4 = 1.75$ eV has energy less than the applied bias (1.8 V), it is not resolved in the LESTM spectrum. This is due to the relative suppression of emission from the higher energy modes, as explained in the previous section. The simulation results indicate a further significant red-shifting of the LSP resonances, with increasing R and the lowest order mode now at 1340 nm.

The surface plasmon resonance wavelength of an isolated nanoparticle (~550 nm for Au nanoparticles [25]) is known to red shift when placed in close proximity to a metal substrate, the red-shift increasing with increasing proximity and with nanoparticle radius [26]. The larger red-shifts observed here, even for the smallest nanoparticle with the spectral peak at 900 nm, are a combined effect of the nanoparticle–substrate proximity ($d = 0.6$ nm) and a *local* reduction in $\hbar\omega_p$ for Au (3.6 eV as used in the simulations). Within the Drude model this reduced value of $\hbar\omega_p$ can be interpreted as an effective lowering of the average density of conduction electrons. For two metal bodies within tunnelling proximity, their large background polarizability with the large electric fields involved lead to surface charge screening, constraining the number of free electrons available to participate in LSP oscillations [21]. This effect would be restricted to the immediate vicinity of the nanocavity. On the other hand, indications are that for $\lambda > 600$ nm the intrinsic optical properties of isolated Au nanoparticles show limited deviation from bulk values [27].

A comparison of the simulated data (figures 2–4) clearly shows a systematic red shifting of LSP resonances with increasing nanoparticle radius. Thus tip/nanoparticles of larger radii can sustain lower energy LSP modes, or conversely for nanoparticles of smaller radii the excited modes are constrained to higher energies. The LESTM spectrum B in figure 4 shows the emission from a tip of $R \sim 100$ nm recorded with an InGaAs detector, from [21]. The spectral peak at 1470 nm corresponds to the lowest order LSP mode. Compared with the simulation for the 80 nm nanoparticle, the mode has shifted further into the infrared. The peak at 950 nm corresponds to the second order resonance and the shoulder centered at 1072 nm to the first order resonance, both of which have red shifted in line with the above discussion. Unfortunately, current computational capabilities available to us restricts modelling to nanoparticles of $R < 80$ nm.

The above results also show that increasing R increases the number of LSP modes excited, with the E_f assuming a more broadband nature. The unnormalized E_f shows that its overall magnitude increases monotonically with R with the maximum E_f increasing four fold between $R = 10$ and 80 nm, indicating a stronger electromagnetic coupling of the nanoparticle–sample system for larger radii [19]. These features are highly pertinent to the design of any junction-based optical spectroscopy. To optimally exploit the LSP mediated enhancement effects a spectral region of large field enhancement (preferably an LSP resonance) should span the relevant energy range of interaction of any sample placed in the nanocavity. Thus, the broader the line-width of the LSP modes or the higher the uniformity (across λ) of the overall enhancement of a junction, the greater is its applicability to a varied range of molecules. Further in the context of LESTM, by judiciously choosing the sample bias we can progressively select and excite LSP modes starting from the long wavelength end of the spectrum, thus tuning the probe to the energetics of the sample in question.

A crucial aspect of both TERS and LESTM spectroscopy is the lateral resolution afforded by the techniques. This is determined by the spatial variation of the electric field within the nanocavity, specifically in the xy plane. For the case of the $R = 80$ nm nanoparticle, figures 5(a)–(e) show a series of 2D plots of E_f across a 30 nm square xy plane, positioned 0.1 nm directly below the nanoparticle. The snapshots at five specific wavelengths (600, 700, 800, 900 and 1200 nm) clearly show an extremely non-uniform oscillatory electric field in the nanocavity progressively decaying with increased distance from the system axis. The oscillations are most evident at shorter wavelengths with the secondary peaks shifting towards the system axis with decreasing wavelength. Supplementary data include an animated gif (SD1.gif) showing the evolution of the above xy plot over the entire wavelength range.

The asymmetric nature of E_f (figure 5) along the x-direction is a consequence of the asymmetry in the incidence of the excitation field. Figures 6(a)–(c) show plots of normalized E_f (along the line shown in figure 5(b)) at specific wavelengths (see above) for nanoparticles of radii 80, 25 and 10 nm. The oscillatory variation of E_f with distance from the system axis is a feature specifically associated with the *proximity* of the nanoparticle to a *metallic* substrate. This is clearly demonstrated by comparison with the case where the substrate is replaced with a *dielectric* medium, SiO_2, as shown in figure 5(f); this is simulated for the same parameters as for figure 5(a) but with the substrate having a refractive index of 1.45. The contrast is further elucidated in figure 5(g), which plots the normalized E_f from figures 5(a) and (f) along the line $x = 0$. For the case of SiO_2, the lateral variation assumes a broader, typically Gaussian profile [9, 15]. At $\lambda = 600$ nm the magnitude of E_f for the Au substrate is ~7 fold stronger than for the SiO_2 substrate. The stronger enhancement and the oscillatory variation of E_f observed for an Au substrate originates with a stronger resonant coupling between the nanoparticle LSPs and the propagating plasmons of the substrate surface.

Figure 6 shows that the central peak width is a function of both R and λ. However, the presence of the secondary peaks (and their decay length scale) significantly affects any calculation of the lateral resolution. It is worth noting that for a specific nanoparticle the peak to peak separation (s_{pp}) is found to increase monotonically with λ (see supplementary data: file SD2.jpg). s_{pp} varies from 3 nm at $\lambda = 600$ nm to 22 nm at 1200 nm for the 80 nm nanoparticle, while for the 10 nm nanoparticle s_{pp} varies from 1.5 nm at 600 nm to >10 nm at 900 nm. The field profiles shown above and s_{pp} values are not only important in determining the lateral resolution but also relevant to nanoparticle assisted lithography applications, where the near-field enhancement below nanoparticles is directly used to pattern the underlying substrate [9].

Figure 7 plots the normalized E_f value at the peak positions for the various excitation wavelengths

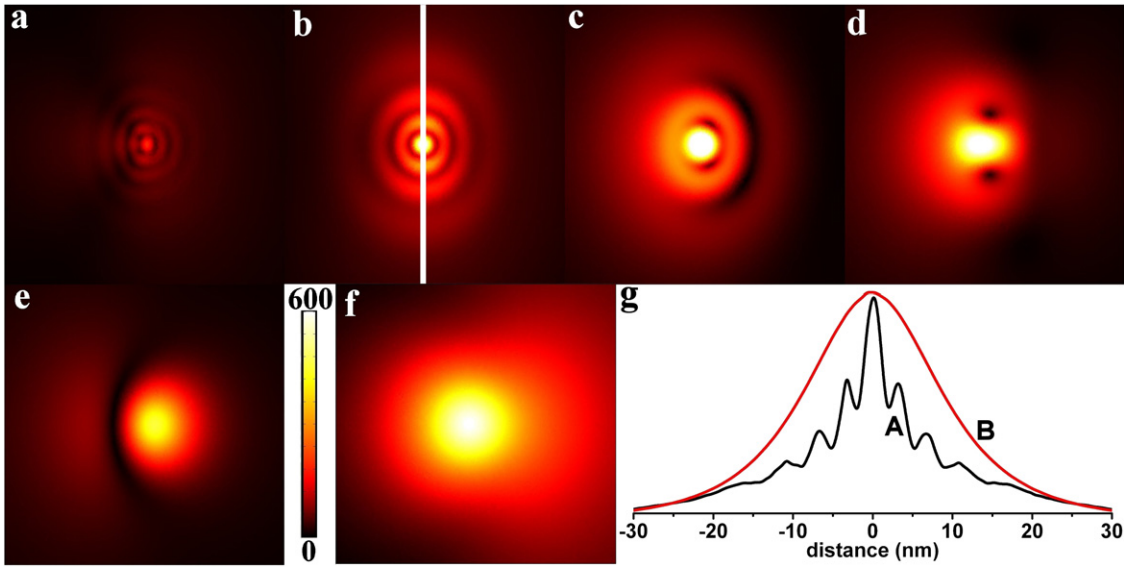

Figure 5. (*a*)–(*e*) 30 × 30 nm^2 plot of E_f on the *xy* plane, centred 0.1 nm below an Au nanoparticle ($R = 80$ nm), with an Au substrate, for $\lambda = 600$ nm, 700 nm, 800 nm, 900 nm and 1200 nm, respectively. The same colour scale shown is used for (*a*)–(*e*). (*f*)—same as (*a*), but with the SiO_2 substrate (colour scale is ×15 that of (*a*)–(*e*)). (*g*) Plot of normalized E_f (along the line $x = 0$ depicted in (*b*)). A: for image (*a*) and B: for image (*f*).

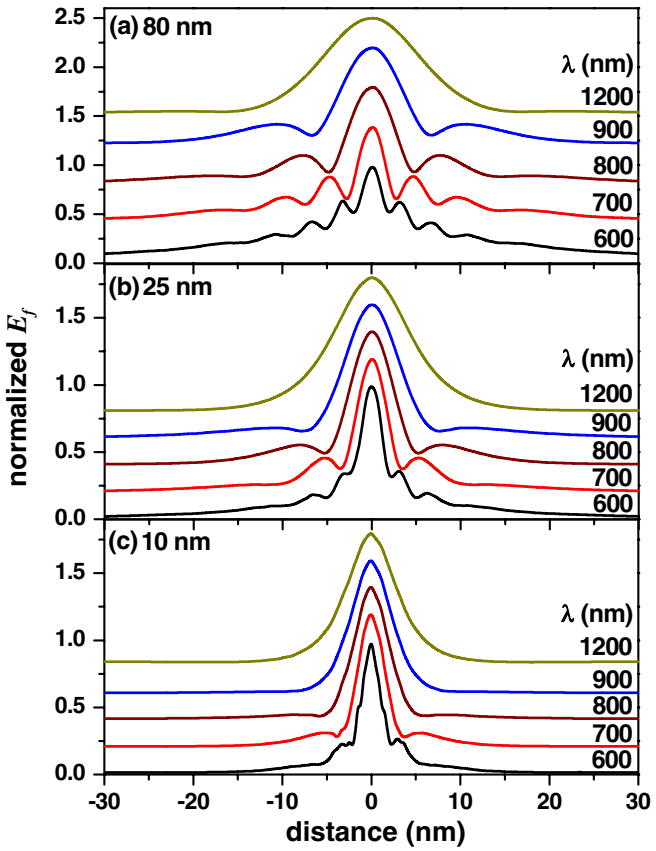

Figure 6. Normalized E_f plotted along the line shown in figure 5(*b*) for nanoparticle radii (*a*) 80 nm, (*b*) 25 nm and (*c*) 10 nm for various values of λ. Individual plots are vertically shifted for clarity.

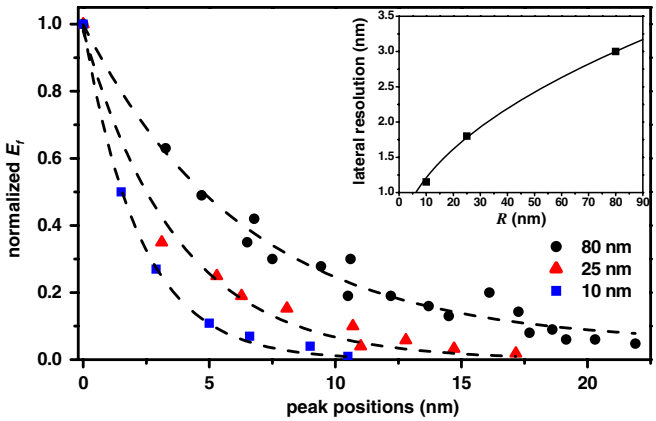

Figure 7. Dependence of the normalized peak electric field values with peak positions for nanoparticles of radius $R = 10$, 25 and 80 nm; the dashed lines indicate fits to first order exponential decay. The inset shows the calculated lateral resolution as a function of nanoparticle radius and the fitted line indicates a $R^{1/2}$ dependence (see text).

$600 \leqslant \lambda \leqslant 1200$ nm for all three nanoparticles and is used to determine the lateral resolution. The peak E_f values follow a first order exponential decay (dashed curves in figure 7). The decay length is primarily governed by the geometric properties of the nanocavity (parameters R and d) and, as expected, is least for the smallest nanoparticle. Interestingly, there is negligible wavelength dependence within the range probed. For TERS the lateral resolution is determined by the variation of the fourth power of E_f and has been discussed extensively in the literature [13, 15]. Here, in the context of LESTM, we calculate the lateral resolution as the distance at which $|E_f|^2$ falls to 50% of its central maximum. It is calculated from the square of the fits of first order exponential decay shown in figure 7. The variation of this calculated lateral resolution with nanoparticle radius is shown in the inset to figure 7. A fit to the lateral resolution values closely follows a $R^{1/2}$ dependence that mimics the LSP localization length dependence on R predicted earlier [17]. However, even for the $R = 10$ nm nanoparticle,

the lateral resolution ∼1.2 nm and the simulations predict sub-nanometre resolution only with tips of $R < 5$ nm.

The above analysis of achievable lateral resolution pertains to LSPs and the local variation in the electromagnetic coupling. Variation in the electronic structure may occur on a more localized scale and be a sufficiently dominant influence to yield higher resolution optical contrast. Thus Hoffman *et al* [28] explain the contrast in atomically resolved photon maps (on Au(1 1 1) surface) purely in terms of local variation in electron tunnelling probability, neglecting any lateral variation in electromagnetic coupling.

4. Conclusions

In conclusion, we have performed finite element calculations of the electric field enhancement in an Au nanoparticle–substrate nanocavity as a function of wavelength and nanoparticle radii. The calculated LSP modes of the nanocavity can be experimentally excited and analysed by recording the LESTM spectra from Au tips of comparable radii. Agreement between the calculated LSP modal energies and those obtained experimentally dictates a reduced effective bulk plasma frequency for Au. The simulation results also show that with increasing nanoparticle radii the LSP modes systematically red shift and the overall electric field enhancement increases significantly in magnitude with an almost broadband enhancement shown for the largest nanoparticle ($R = 80$ nm). In contrast to earlier reports, the lateral variation of the electric field in the nanocavity is found to be oscillatory in nature with an exponential lateral decay. The feature is a consequence of the tunnelling proximity of the nanoparticle–substrate system and is uniquely associated with the metallic nature of the substrate. The spatial resolution is shown to be primarily governed by the geometric properties of the nanocavity and is limited to the supra-nanometre scale even for the smallest nanoparticle investigated. Sub-nanometre resolution is predicted for still sharper tips of end radius <5 nm.

Acknowledgments

The authors thank Mr Anthony Murphy for helpful discussions regarding COMSOL. They acknowledge the financial support from the UK Engineering and Physical Sciences Research Council and 'Nanotec Northern Ireland' supported by EC funding through Invest Northern Ireland.

References

[1] Nie S and Emory S R 1997 *Science* **275** 1102
[2] Acimovic S S, Kreuzer M P, Gonzalez M U and Quidant R 2009 *ACS Nano* **3** 1231
[3] McFarland A D and Van Duyne R P 2003 *Nano Lett.* **3** 1057
[4] Boisselier E and Astruc D 2009 *Chem. Soc. Rev.* **38** 1759
[5] Boyle G M, Mitra J and Dawson P 2009 *Nanotechnology* **20** 335202
[6] Wijaya A, Schaffer S B, Pallares I G and Hamad-Schifferli K 2009 *ACS Nano* **3** 80
[7] Ono A, Kato J-I and Kawata S 2005 *Phys. Rev. Lett.* **95** 267407
[8] Heltzel A, Theppakuttai S, Chen S C and Howell J R 2008 *Nanotechnology* **19** 025305
[9] Eversole D, Luk'yanchuk B and Ben-Yakar A 2007 *Appl. Phys. A: Mater. Sci. Process.* **89** 283
[10] Steidtner J and Pettinger B 2008 *Phys. Rev. Lett.* **100** 236101
[11] Anderson N, Hartschuh A, Cronin S and Novotny L 2005 *J. Am. Chem. Soc.* **127** 2533
[12] Downes A and Welland M E 1998 *Phys. Rev. Lett.* **81** 1857
[13] Downes A, Salter D and Elfick A 2006 *J. Phys. Chem.* B **110** 6692
[14] Micic M, Klymyshyn N, Suh Y D and Lu H P 2003 *J. Phys. Chem.* B **107** 1574
[15] Notingher I and Elfick A 2005 *J. Phys. Chem.* B **109** 15699
[16] Le F, Lwin N Z, Steele J M, Kall M, Halas N J and Nordlander P 2005 *Nano Lett.* **5** 2009
[17] Rendell R W and Scalapino D J 1981 *Phys. Rev.* B **24** 3276
[18] Gozhenko V V, Grechko L G and Whites K W 2003 *Phys. Rev.* B **68** 125422
[19] Johansson P 1998 *Phys. Rev.* B **58** 10823
[20] Boyle M G, Mitra J and Dawson P 2006 *Japan. J. Appl. Phys. Part 1* **45** 2119
[21] Boyle M G, Mitra J and Dawson P 2009 *Appl. Phys. Lett.* **94** 233118
[22] Born M and Wolf E 1964 *The Principles of Optics* (Oxford: Pergamon)
[23] Etchegoin P G, Ru E C L and Meyer M 2006 *J. Chem. Phys.* **125** 164705
[24] Boyle M G, Feng L and Dawson P 2008 *Ultramicroscopy* **108** 558
[25] Muller J, Sonnichsen C, von Poschinger H, von Plessen G, Klar T A and Feldmann J 2002 *Appl. Phys. Lett.* **81** 171
[26] Okamoto T and Yamaguchi I 2003 *J. Phys. Chem.* B **107** 10321
[27] Stoller P, Jacobsen V and Sandoghdar V 2006 *Opt. Lett.* **31** 2474
[28] Hoffmann G, Maroutian T and Berndt R 2004 *Phys. Rev. Lett.* **93** 076102